

Analyzing the speed of sound in neutron star with machine learning

SAGNIK CHATTERJEE ¹, HARSHA SUDHAKARAN ¹, AND RITAM MALLICK ¹

¹ *Department of Physics
Indian Institute of Science Education and Research Bhopal
Bhopal, Madhya Pradesh
462066, India*

ABSTRACT

In this work we have analyzed the variation of speed of sound and trace anomaly inside a neutron star using neural network. We construct family of agnostic equation of state by maintaining thermodynamic stability, speed of sound bound with constraints from recent observation of neutron stars. The data of mass and radius serves an input for the neural network and we obtain speed of sound as an output. The speed of sound shows non-monotonic behaviour and the trained data predicts softer equation of state. The neural network predicts stiff equation of state at the centre of intermediate mass stars and massive stars have relatively softer equation of state at their centre. The trace anomaly shows a non-monotonic behaviour for the untrained data however, when we train our data; with neural network the trace anomaly shows monotonic behaviour and the condition of $\Delta \geq 0$ is maintained.

1. INTRODUCTION

Matter at Neutron star (NS) cores are at highly compressed state and due to gravity the density can built up to few times nuclear saturation density. They are very compact and has been observationally identified with pulsars with their mass being in the range from 0.7 – 2.1 solar masses (Valentim et al. 2011) and radius between 10 – 15 km. They are therefore one of the best laboratories to test the theory of strong interaction at high density low temperature regime. One of the most interesting facts of QCD is the conjecture of a phase transition (PT) (Witten 1984) from hadronic matter (HM) to quark matter (QM) at these densities (Shuryak 1980). This has led to extensive experimental/observational and theoretical effort to understand the matter properties at neutron star interiors. The field got a huge boost after several precise mass measurement of massive pulsars (Riley et al. 2019; Riley et al. 2021; Miller et al. 2019; Miller et al. 2021) and the gravitational wave (GW) observation of binary NS mergers (BNSM) (Abbott et al. 2017). Although in the last few years we have been able to constrain the matter properties (equation of state (EoS)) still our knowledge about the EoS at such densities is limited.

The first principle calculation of matter at low density (till saturation density) (Hebeler et al. 2013) and at asymptotic high density are possible (Lattimer & Prakash 2004), but for intermediate densities they are still beyond our reach. Physicist have either relied on

models or used agnostic approaches to understand matter at intermediate densities which are found at the cores of NSs (de Forcrand 2010). The agnostic approach fails to have any microscopic detail of the matter; however, the overall properties of the NS can be obtained from them. Whatever may be the approach, the models has to satisfy the constraints obtained from theory and observations. EoS obtained from agnostic approach are based on methods like Bayesian analysis and machine learning to predict the most probable EoS. Bayesian analysis are extensively used nowadays to impose constrains from observational data like in BNSM (Most et al. 2018; Annala et al. 2018; Zhang et al. 2018). They are basically statistical or probabilistic models that account for uncertainty in measurements.

With the current constraints from observational astrophysics of neutron stars and from the agnostic models one can restrict the EoS to a certain limit. To constrain the EoS one needs a good parameter to build the agnostic model. One of the parameter is the adiabatic speed of sound (c_s), which relates the density and pressure of the EoS (Bedaque & Steiner 2015). As it is defined as the first derivative of pressure with respect to energy density; it refers the amount of matter that can be accommodated for a particular pressure so that it can balance the gravitational pull. This is the measure of the stiffness of the EoS. The sound speed is constrained in the range between 0-1 which comes from hydrostatic equilibrium and causality. Large sound speed refers to larger stiffness and thereby massive stars. The

sound speed is also bounded at asymptotic densities by perturbative-QCD (pQCD) calculations which predicts that the sound speed square should asymptotically reach the value $1/3$ (Komoltsev & Kurkela 2022). However, it should be emphasized that in the intermediate densities the sound speed could breach this value and it had been shown that it should be necessary to generate massive stars (Kojo 2021; Altiparmak et al. 2022).

There are many formulations by which one can obtain the EoS using the constraints in the speed of sound. One of such method is the machine learning (ML). ML has been already in use to study NS properties (Fujimoto et al. 2018, 2020, 2021; Morawski, F. & Bejger, M. 2020; Krastev 2022; Soma et al. 2022). Optimal speed of sound can be obtained by using ML approach considering the observational constraints and mass-radius measurements of pulsars. Supervised ML can be used in mapping the non-linear mass radius relation to speed of sound. The non-linear mapping is done by the neural network (NN) which use the mass-radius uncertainty to first learn the map and then predict the sound speed. The data are prepared in a model independent way from observations and then fed into the neural network. Having a good amount of data can minimize the error in predicting the correct speed of sound and can be independent of any unintended bias. In this work we first randomly build agnostic EoS from the sound speed and NS observational constraints and prepare our data from several mass and radius measurement of observed pulsars. The mass-radius data is used as an input to find the speed of sound as an output from the NN. The speed of sound is then used to obtain the matter properties at NS cores.

The paper is arranged in the following way : Section 2 gives the formalism of our work which explains the data preparation and the formulation of the NN. Next, in section 3 we show our results. Finally, section 4 summarizes the work and draws important conclusions.

2. FORMALISM

In this article our main aim is to predict the speed of sound inside the neutron star using ML. One of the main bottleneck of using ML is the need of a huge amount of data to have reliable results. We will first construct a huge number of agnostic EoSs in this article by randomizing the speed of sound in the density range where it is not known. We then implement NS mass radius measurement to constrain the data. However, this is a problem in the sense that the simultaneous measurement of NSs mass and radius are very limited and also involves considerable error. To fix this we employ the procedure followed by Fujimoto et al (Fujimoto et al. 2018) where

we introduce considerable error in the mass radius measurement. The data generation starts with constructing an enormous amount of agnostic EoS satisfying the thermodynamic stability criterion and respecting the condition that the speed of sound is bounded in the range $0 \leq c_s \leq 1$. The EoS at the low density regime and high density regime is constrained with BPS EoS and pQCD calculation simultaneously.

2.1. Data Preparation

To begin with the process of preparation of data, we randomly generate 80,000 agnostic EoSs. This is done by taking BPS crust EOS (Baym et al. 1971) till a density of $n \leq 0.57n_0$ ($n_0 = 0.16 fm^{-3}$ being the nuclear saturation density) . From this density to a density $1.1n_0$, we take either "stiff" or "soft" EoS (Hebeler et al. 2013; Keller et al. 2021; Epelbaum et al. 2009; Tews et al. 2013) spanning the chiral effective theory (CET) band. Corresponding to the saturation density, the energy density is defined as ϵ_0 . From ϵ_0 to $8\epsilon_0$, we randomize the square of the speed of sound (c_s^2) with five equal spacing assuming that the maximum density that a star can attain (for any EoS) can be at most be 8 time saturation density. Beyond $8\epsilon_0$ we randomize the speed of sound at four points which are $20\epsilon_0, 40\epsilon_0, 60\epsilon_0$ and $90\epsilon_0$. The value of c_s cannot exceed the causal limit and cannot be less than zero. Hence, we take the range as $0.0 \leq c_s^2 \leq 1$. As $c_s^2 = (\partial P / \partial \epsilon)_s$, where P is the pressure and ϵ is the energy density; hence we perform a linear interpolation at each of these intervals to obtain the entire profile of the EoSs. At asymptotically high densities, our EoSs follow the conformal field theory and $c_s^2 \rightarrow 1/3$ (Kurkela et al. 2010; Gorda et al. 2018; Altiparmak et al. 2022).

We created 80,000 such EoSs as shown in Fig 1. Although the EoS are thermodynamically stable we need to check whether they are also consistent with the current observational constraints. To apply the current observational constraints, we need to solve the Tolman-Oppenheimer-Volkoff equation (TOV) (Oppenheimer & Volkoff 1939) and generate mass-radius (M-R) sequence. From these M-R sequences we reject those EoSs having maximum mass $M_{TOV} < 2M_\odot$ imposed by the mass measurements of J0348+0432 (Antoniadis et al. 2013) ($M = 2.01 \pm 0.04 M_\odot$) and J0740+6620 (Cromartie et al. 2020) ($M = 2.08 \pm 0.07 M_\odot$). In addition, we further reject those EoSs with $R < 10.75 km$ at $M = 2M_\odot$ and $R < 10.8 km$ at $M = 1.1M_\odot$ imposed by the NICER constraints of J0030+0451 (Riley et al. 2019; Miller et al. 2019) and J0740+6620 (Riley et al. 2021; Miller et al. 2021). The next constrain comes from the radius measurement of J0030+0451 having radius of $12.33 \pm_{0.81}^{0.56} km$ (Raaijmakers et al. 2021). We have also used the con-

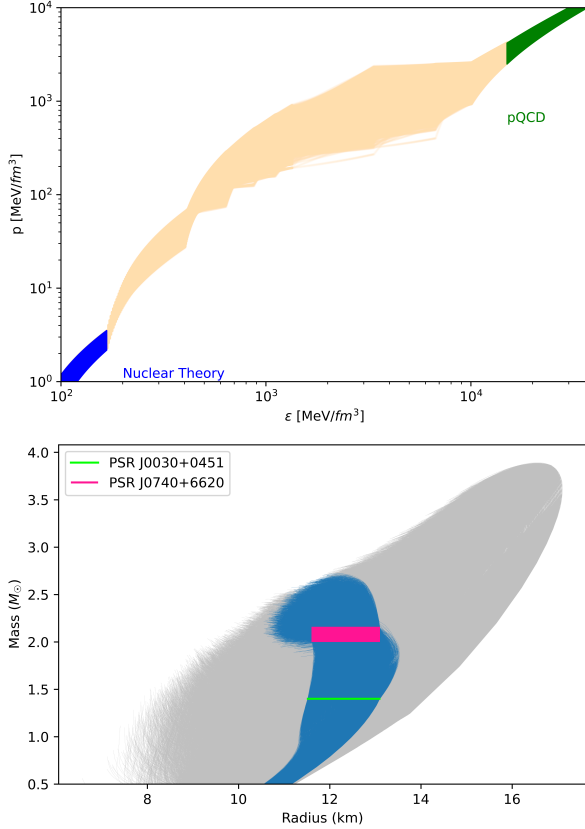


Figure 1. (Top): The plot for the pressure vs energy density for 12195 EoS. The green colored band represents the pQCD band, and the blue colored band denotes the CET band. The peach colored lines denotes the EoSs generated using randomization of speed of sound. **(Bottom):** The M-R curve showing the EoSs following the NICER constraints. The gray colored lines are the ones which are rejected after imposing constraints. The blue colored lines (12,195) represents the ones, which follows the constraints and are then used for further analysis. The two constraints are also shown in the figure.

straints from J0740+6620 ($2.08 \pm 0.07 M_{\odot}$) which has a radius of 12.35 ± 0.75 km (Miller et al. 2021). We were left with only 12,195 EoSs after imposing the following constraints. These two constraints on the M-R diagram is shown in the figure 1. The radius constrain of the higher mass stars makes the plot to bulge. In this work, we have not imposed the strict conditions on tidal deformability (Hinderer et al. 2010). This is done to have enough EoS for training and testing our Neural network.

Next, we segregate our EoSs, into training-set(9,195 EoSs) and test-set (3,000 EoSs), respectively. Theoretically generated EoS has a smooth sequence stretching from very low mass to the maximum mass. Also there is no uncertainty in the mass and radius for a given EoS. However, observationally both the mass and radius

measurement are accompanied with errors. To build the training data from the constructed EoS we need to incorporate the errors in our data which would eventually not define a point but rather a region. For training our NN, we select 15 points on the MR curve for each EoSs. we then introduce errors in each of the points. The amount of errors in the measurement of mass and radius is sampled from the normal distribution with standard deviation $0.1 M_{\odot}$ and 0.5 km respectively (Fujimoto et al. 2018, 2021). This is shown in fig 2. For each EoS, this process is repeated for 100 times, and we produce a total of 919,500 data points for training our NN.

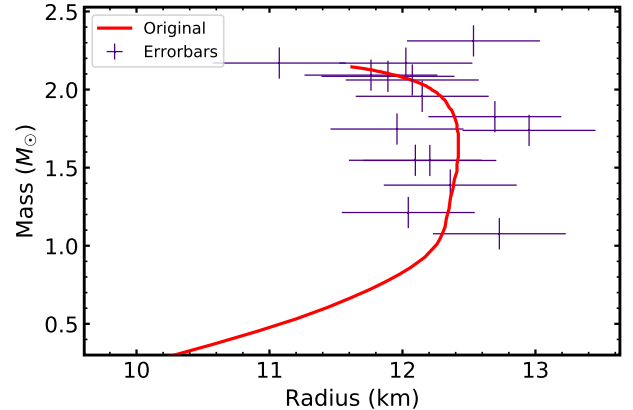


Figure 2. The following figure shows how we sample 15 random points on the MR curve of our EoS and then randomly sample and shift each of those 15 points

2.2. Neural Network

The measurement of the maximum mass, along with NICER and LIGO observation of NS has put severe constraints on the EoS; however, the most likely EoS for high density matter mostly at the intermediate region is far from being determined with relative confidence. In the last few years there has been continuous effort to extract the most likely EoS and one of the most used method to determine them is using Bayesian Analysis (Raithel et al. 2017; Lim & Holt 2019; Char et al. 2020; Biswas 2022). However, it has its restriction due to the lack of knowledge of the prior distribution. There has also been methods employing ML using NN for determining the likely EoS (Fujimoto et al. 2018; Morawski, F. & Bejger, M. 2020). In this article we employ ML methods using NN (Goodfellow et al. 2016); however we use speed of sound inverse mapping to find the EoS. We use the mass-radius data (obtained from the previous subsection) as an input to the neural network to obtain the c_s^2 for the five segments (ϵ). From the c_s^2 obtained

from the NN we then find the corresponding pressure and thereby recreating the ML predicted EoS.

The NN structure has an input layer with 30 neurons, that takes 15 randomly sampled pairs of M and R as input. Subsequently we have three hidden layers each having 40 neurons. The final layer has 5 neurons which gives us the c_s^2 as output as shown in fig 3 and represented in table 1. Since the maximum central density of the NSs lies in the range of ϵ_0 to $8\epsilon_0$, we take the output neuron to be 5, which is equivalent to the number of segments made while constructing our EoSs. The data obtained after sampling is split into training and validation data. About 80 percent being the training data and the rest 20 percent being the validation data. The model learns the relevant parameters from the training data and its performance is evaluated on the validation data. The data points are normalized with $3M_\odot$ for mass and 20km. This normalisation speeds up the learning procedure and as a result the loss function converges faster. Also training data is prepared with data points having mass greater than $1M_\odot$. Loss function is the difference between actual output and predicted output. For our model, we take MSE (mean squared logarithmic error) as our loss function which is optimised using Adam (Kingma & Ba 2014). Adam tends to converge faster and performs better than other optimisation algorithms. The activation function for hidden layers is ReLU (Rectified Linear Unit) as ReLU is easier to train with and avoids vanishing gradient problem. For the output layer, activation function is \tanh . \tanh returns values in the range from 0 to 1 for positive inputs therefore can be used for predicting c_s^2 which also lies in the same range. Our model converges to a training loss of 0.0214 and mean squared error of 0.0462 at the end of 1000 epochs as shown in fig 4. Our model is built using the Python Keras (Chollet et al. 2015) with TensorFlow (Abadi et al. 2015). Here the architecture used is similar to the one used by (Fujimoto et al. 2018). Our results were performed over different layer sizes with different learning rates. The results documented here are the optimal ones giving the minimum value of MSE.

3. RESULTS

Once we have described our formalism of constructing the agnostic EoS and building the data we then feed the data to the neural network to obtain the speed of sound for 5 points within the star (4 at much larger densities are obtained by interpolating them). From the speed of sound and for a given segment (in ϵ) we linear interpolate to obtain the machine learned EoS. The machine learned EoS is then solved to obtain mass-radius curve. Fig 5 shows the nature of the MR curve after train-

Layer	Neurons	Activation
Input Layer	30	None
Hidden Layer 1	40	ReLU
Hidden Layer 2	40	ReLU
Hidden Layer 3	40	ReLU
Output Layer	5	tanh

Table 1. This table explains the structure of our neural network. The input layer contains 15 neurons. The subsequent three hidden layers each contain 40 neurons with activation as ReLU. The output layer has 5 neurons with \tanh as the activation function

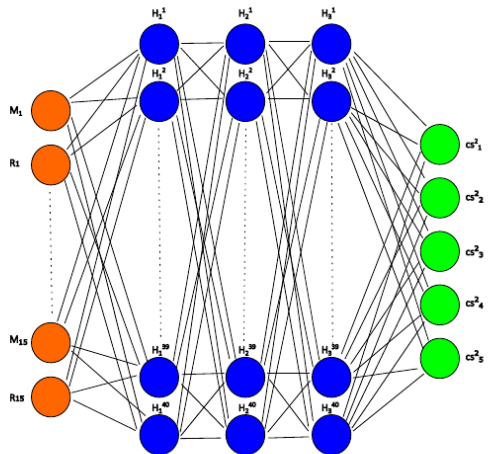


Figure 3. A schematic diagram of the structure of our NN. The input layers are shown with orange colors, with $M_1, M_2 \dots M_{15}$ and R_1, R_2, \dots, R_{15} are the 15 pairs of mass and radius which we provide as input for our NN. The nodes of the hidden layer are shown with the blue color and each hidden layer is marked as 'H'. The final output layers are represent by green color having five c_s^2 as the outputs.

ing our network for a single EoS. The red colored line indicates the original nature of the MR, and after training our NN, the resultant MR is given by the blue line. The machine learned MR curve deviates from the original curve (mostly for stars of higher mass) because of the error introduced from the measurement. This shows that the NN works well and does not overfits the data.

Once we have checked that it works well for several EoS we then plot the c_s^2 as function of ϵ . In fig 6 the variation of c_s^2 against the density ϵ is shown. The plot shows the variation for both the trained (represented by pink) and untrained (represented by cyan) datasets. We have trained our system (for NN) till $8\epsilon_0$ and obtained the speed of sound as an output from the NN. This is because the measurement constraints are only

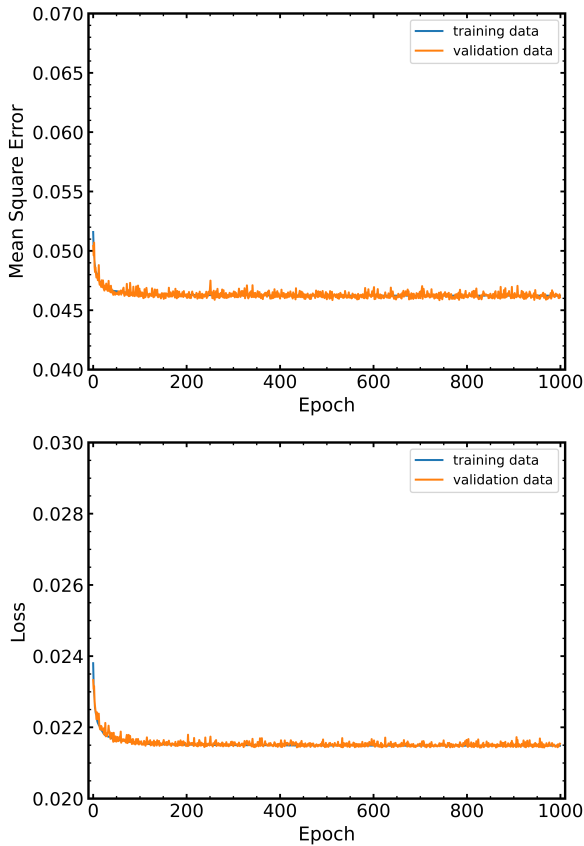


Figure 4. (Top): Plot for MSE (Mean square logarithmic error) against epochs. The blue colored line represents the change in mean squared error for training data whereas the orange colored line represents the change in mean squared logarithmic error for validation data upto 1000 epochs. **(Bottom):** Plot for Loss against epochs. The blue colored line represents the change in mean squared logarithmic error for training data whereas the orange colored line represents the change in mean squared error for validation data upto 1000 epochs.

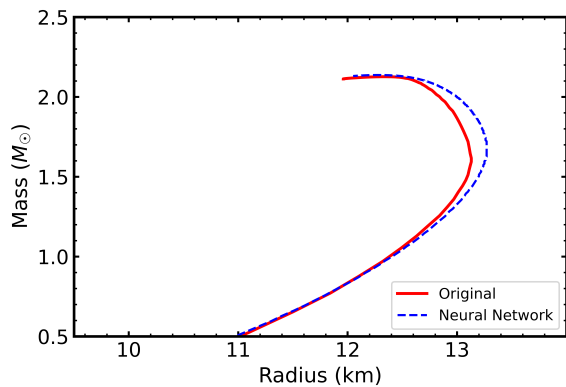


Figure 5. The MR curve after training. The red colored line shows the original MR curve and the blue colored dotted line shows the MR curve which we obtain after training.

upto NS central densities which for all the cases does not cross $8\epsilon_0$. Beyond $8\epsilon_0$ we continue with the agnostic speed of sound. This is also clear from the figure as beyond $8\epsilon_0$ the pink and cyan curves coincides. Starting from the low density we find that in the first slice $\epsilon_0 \leq \epsilon \leq 2.4\epsilon_0$ the speed of sound remains less than the conformal sound speed for both the trained and untrained set. This is expected as the sound speed is directly related with the stiffness of the EoS. High sound speed at such densities would indicate that for most of the stars the EoS is most stiff at the outer regions, which is counter-intuitive.

The speed of sound reaches a maximum value mostly in the second slice which is the central density of most of the intermediate massive stars. It is interesting to note that that both for the trained and untrained data there is a first peak at around $(3.2 - 3.3)\epsilon_0$. For the trained data the maxima of the sound speed is less than that for untrained data. Therefore, the neural network predicts less stiffer EoS at the centre of most of the intermediate stars. In the next slice the trained and untrained data differs maximally. There is a minima for the trained data at around $5\epsilon_0$, which is the central density of stars with mass around 2 solar mass (there can be some deviation for the mass depending on the EoS). However, the untrained data do not show such sharp minima. Therefore, the trained data predicts that stars whose masses are about 2 solar mass have the matter EoS as the stiffest in the intermediate region and the core has a relatively softer matter. For the trained data (the mean) have a second peak at around $7.4\epsilon_0$. Such high density are very rare in NS and only extraordinarily massive NSs (and only a handful EoS) can reach this density. Such stars have alternating softer and stiffer region in their interior.

Another interesting thing to note is that beyond $10\epsilon_0$ both the trained and untrained data coincides as we are not training our data beyond $8\epsilon_0$ as there are no observational or theoretical constrain in this region. However, at asymptotically high density they should converge to the conformal sound speed ($c/3$). The mean of the sound speed converge to the conformal value however, before it does the sound speed becomes less than the conformal value and then rises.

A similar study using bayesian analysis is done by Altıparmak et al recently (Altıparmak et al. 2022), and our results are quite similar to their work. For our case the peak is slightly shifted towards the right; this is because, in our approach of constructing the EoSs, we have considered the energy densities at fixed intervals. In (Altıparmak et al. 2022), they have randomized the densities. We could not adapt their approach as we re-

quire densities at fixed intervals for our NN; randomizing the densities would not have served the purpose.

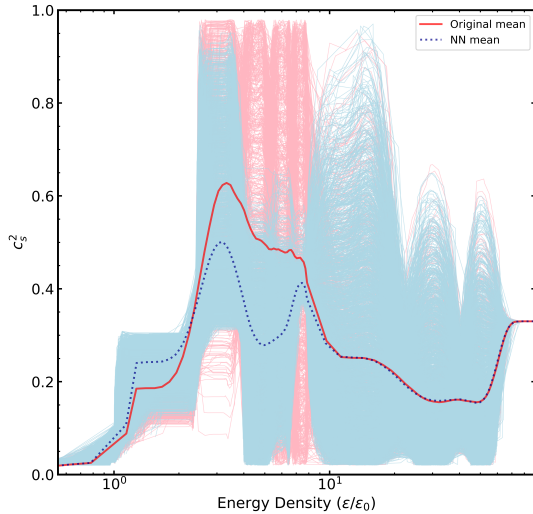


Figure 6. The plot for the square of the speed of sound against the density of the star. The pink colored lines represents the plots for 3000 randomly selected untrained EoSs. The cyan colored lines are the plots for the same EoSs after they have been trained.

It would be insightful to plot the variation of c_s^2 inside the star to know more about the exact nature of the matter inside the star. In fig 7 (top) and fig 7 (bottom), we show the variation of the speed of sound inside the NS for stars of masses $1.6M_\odot$ and $2.2M_\odot$ respectively. In our plots, the red-colored density distribution is for the untrained datasets and blue for the trained datasets. Their respective means are also shown by red and blue colored lines. For the star with 1.6 solar mass the sound speed is maximum at the centre and then decreases slowly with radius. This is because the central density of the star is such that the sound speed still has not reached its peak (fig 6). After 4 km it falls off sharply and reaches a plateau like region between 7 – 11 km. This correspond to the typical plateau region of fig 6 at the low density part. Ultimately near the surface the sound speed falls off to almost zero. However, the sound speed plot for $2.2M_\odot$ star is a bit different in the central region. As such stars have central density around $5\epsilon_0$ (beyond the peak density of sound speed), initially the speed of sound is less at the centre and has a maximum at around 7 km and then it falls off as we go further towards the surface of the star (including the plateau region). As evident from the fig 6 the trained data shows that the mean sound speed is less than that of the untrained data. The NN predicts relatively softer EoS than one obtains from agnostic EoS.

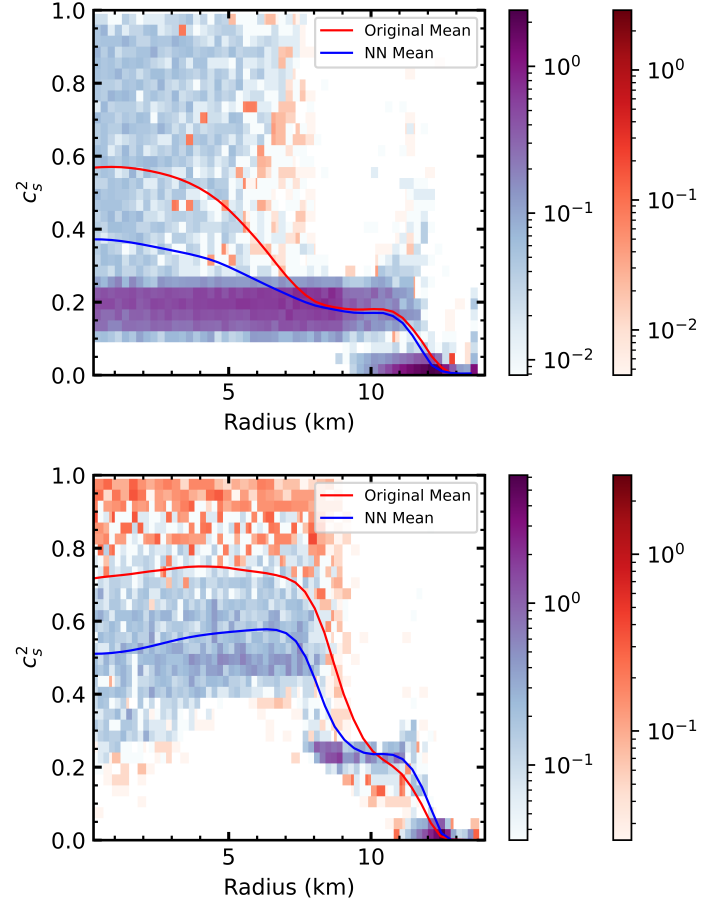


Figure 7. (Top): The density plot for the square of the speed of sound against the radius from center to the surface of a $1.6M_\odot$ star. The red color denotes the untrained EoSs, and the blue color denotes the trained EoSs. The red and blue colored are their means respectively. **(Bottom):** The plot for the square of the speed of sound against the radius from center to the surface of a $2.2M_\odot$ star. The nomenclature remains the same.

A similar analysis (not considering the NN approach) for $1.4M_\odot$ and $2M_\odot$ was done by Ecker et al (Ecker & Rezzolla 2022a). Our results are qualitatively similar to what they have obtained.

3.1. Trace anomaly

QCD in the massless limit shows conformal symmetry and the expectation value of the trace of the energy-momentum tensor $\langle T_\mu^\mu \rangle$ in the classical level becomes zero. For matter at finite temperature and/or chemical potential $\langle T_\mu^\mu \rangle$ can be decomposed into vacuum and matter part. For matter the trace anomaly becomes $\langle T_\mu^\mu \rangle = \epsilon - 3p$. At finite temperature and low density, there is a sharp discontinuity in the normalized trace anomaly at deconfinement transition temperature. This is due to the appearance of the gluonic

degrees of freedom in the system. It would be interesting to check how the trace anomaly behaves for finite density and at low temperature (in this case 0). As the trace anomaly depends on the thermodynamic properties of matter (namely pressure and energy density) it has a close connection with speed of sound.

It has been previously shown that the trace anomaly for an ideal fluid is given by (Ecker & Rezzolla 2022b)

$$\langle T_{\mu}^{\mu} \rangle = \epsilon - 3p. \quad (1)$$

Sometimes a measure of trace-anomaly is defined as

$$\Delta = \frac{\langle T_{\mu}^{\mu} \rangle}{3\epsilon} = \frac{1}{3} - \frac{p}{\epsilon}. \quad (2)$$

It was recently shown that the sound speed can be written in terms of the trace anomaly in terms of the derivative and non-derivative part of the measure (Fujimoto et al. 2022). Fig 8 shows the variation of measure of trace anomaly with energy density for the trained and untrained dataset. The trained ones are represented using cyan-colored lines, with their mean shown in blue dotted lines. The pink colored lines denote the untrained ones, with red-colored solid line representing the mean for the untrained ones. Initially the trace anomaly starts from a high value (near about 1/3) and then decreases as we move to high density. Both the trained and untrained data follows a similar pattern. The untrained trace anomaly goes to negative value beyond $4\epsilon_0$ and stays negative till $15\epsilon_0$. It has a minimum around $8\epsilon_0$ and then increases. Ultimately it tends to the conformal value 0 at very high densities. It approaches zero from the positive side. However, the NN network trained data is significantly different from the untrained data. The measure of trace/conformal anomaly shows somewhat monotonic behaviour after training with the NN and it tends towards zero at high density limit. The value of the trace anomaly remains positive throughout the density range. Our analysis suggests that the bound of $\Delta \geq 0$ is followed for most of the EoS after the training with NN and the mean does not go to negative value. The results are quantitatively similar with the results obtained by Fujimoto et al (Fujimoto et al. 2022).

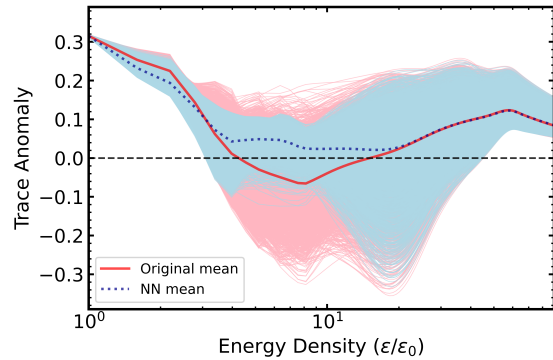


Figure 8. The plot for the measure of trace anomaly against density of for the EoSs. The pink colored lines represents the plots for untrained EoSs. The cyan colored lines are the plots for the same EoSs after they have been trained. The red solid line denotes the mean of the untrained data, and the blue dotted line denotes the mean of the trained data.

4. SUMMARY AND CONCLUSION

In this paper we have studied how the speed of sound and trace anomaly varies with density inside a neutron star. As the intermediate density range is beyond the scope of experiments and direct theoretical calculation we probe the density range with NS observations and constraints. We construct a family of agnostic EoS by maintaining thermodynamic stability and the bound on the speed of sound. After that we filter them by matching with NS observation. We then construct the mass radius curve for these EoS and then we introduce error in both mass and radius which serves as an input for our NN. The neural network gives back the speed of sound in the intermediate density range and then we can linearly extrapolate them to obtain trained EoS.

Doing our analysis we find that at low densities the speed of sound does not cross the conformal limit but rises sharply to a maximum value just beyond $3\epsilon_0$. The trained speed of sound data suggest a lower peak than the untrained one implying a relatively softer EoS. The trained data also has a minimum and a second maxima with the intermediate density range. This is an interesting feature non observed in the untrained data and which suggest non-monotonic speed of sound inside NSs. The non-monotonic speed of sound suggest non-monotonic matter properties inside a NS. Intermediate neutron star has most stiff matter EoS at their centre and then matter becomes softer as we move out of the star. However, massive NSs have relatively softer EoS at their centre and the stiffest EoS lies most in the intermediate region of the star. The untrained data for the conformal anomaly also shows non-monotonicity in their behaviour. It goes to zero at the high density limit; however, the condition of $\Delta \geq 0$ is not always main-

tained in the intermediate region. It goes to negative values even inside the NS. However, when we train the data using NN the measure of trace/conformal anomaly shows monotonicity. It does not go to negative values and the condition of $\Delta \geq 0$ is maintained.

It should be mentioned that in principle the bins for the density range should also be randomized; however, for the NN training this would be difficult. One can also do similar calculation directly relating the EoS with the mass and radius of the star with more sophisticated model like auto encoder. One should also build an order more agnostic EoS and filter them with current NS constraints to check for any biasness towards building the data to be used for training and testing the NN. Also

one expects more constraints from the NICER experiments in the near future which would make such studies more robust.

5. ACKNOWLEDGEMENT

The authors would like to thank IISER Bhopal for providing the infrastructure to carry out the research. SC would like to acknowledge the Prime Minister's Research Fellowship (PMRF), Ministry of Education Govt. of India, for a graduate fellowship. The authors would like to thank Sayan Roy, Kamal Krishna Nath and Shamim Haque for helpful discussions.

REFERENCES

- Abadi, M., Agarwal, A., Barham, P., et al. 2015, TensorFlow: Large-Scale Machine Learning on Heterogeneous Systems. <https://www.tensorflow.org/>
- Abbott, B. P., Abbott, R., Abbott, T. D., et al. 2017, Phys. Rev. Lett., 119, 161101, doi: [10.1103/PhysRevLett.119.161101](https://doi.org/10.1103/PhysRevLett.119.161101)
- Altiparmak, S., Ecker, C., & Rezzolla, L. 2022, The Astrophysical Journal Letters, 939, L34, doi: [10.3847/2041-8213/ac9b2a](https://doi.org/10.3847/2041-8213/ac9b2a)
- Annala, E., Gorda, T., Kurkela, A., & Vuorinen, A. 2018, Phys. Rev. Lett., 120, 172703, doi: [10.1103/PhysRevLett.120.172703](https://doi.org/10.1103/PhysRevLett.120.172703)
- Antoniadis, J., Freire, P. C. C., Wex, N., et al. 2013, Science, 340, 1233232, doi: [10.1126/science.1233232](https://doi.org/10.1126/science.1233232)
- Baym, G., Pethick, C., & Sutherland, P. 1971, ApJ, 170, 299, doi: [10.1086/151216](https://doi.org/10.1086/151216)
- Bedaque, P., & Steiner, A. W. 2015, Phys. Rev. Lett., 114, 031103, doi: [10.1103/PhysRevLett.114.031103](https://doi.org/10.1103/PhysRevLett.114.031103)
- Biswas, B. 2022, The Astrophysical Journal, 926, 75, doi: [10.3847/1538-4357/ac447b](https://doi.org/10.3847/1538-4357/ac447b)
- Char, P., Traversi, S., & Pagliara, G. 2020, Particles, 3, 621, doi: [10.3390/particles3030040](https://doi.org/10.3390/particles3030040)
- Chollet, F., et al. 2015, Keras, GitHub. <https://github.com/fchollet/keras>
- Cromartie, H. T., Fonseca, E., Ransom, S. M., et al. 2020, Nature Astronomy, 4, 72, doi: [10.1038/s41550-019-0880-2](https://doi.org/10.1038/s41550-019-0880-2)
- de Forcrand, P. 2010, PoS, LAT2009, 010, doi: [10.22323/1.091.0010](https://doi.org/10.22323/1.091.0010)
- Ecker, C., & Rezzolla, L. 2022a, The Astrophysical Journal Letters, 939, L35, doi: [10.3847/2041-8213/ac8674](https://doi.org/10.3847/2041-8213/ac8674)
- . 2022b, Monthly Notices of the Royal Astronomical Society, 519, 2615, doi: [10.1093/mnras/stac3755](https://doi.org/10.1093/mnras/stac3755)
- Epelbaum, E., Krebs, H., Lee, D., & Meißner, U.-G. 2009, The European Physical Journal A, 40, 199, doi: [10.1140/epja/i2009-10755-0](https://doi.org/10.1140/epja/i2009-10755-0)
- Fujimoto, Y., Fukushima, K., McLerran, L. D., & Praszalowicz, M. 2022, Phys. Rev. Lett., 129, 252702, doi: [10.1103/PhysRevLett.129.252702](https://doi.org/10.1103/PhysRevLett.129.252702)
- Fujimoto, Y., Fukushima, K., & Murase, K. 2018, Phys. Rev. D, 98, 023019, doi: [10.1103/PhysRevD.98.023019](https://doi.org/10.1103/PhysRevD.98.023019)
- . 2020, Phys. Rev. D, 101, 054016, doi: [10.1103/PhysRevD.101.054016](https://doi.org/10.1103/PhysRevD.101.054016)
- . 2021, Journal of High Energy Physics, 2021, 273, doi: [10.1007/JHEP03\(2021\)273](https://doi.org/10.1007/JHEP03(2021)273)
- Goodfellow, I., Bengio, Y., & Courville, A. 2016, Deep Learning (MIT Press)
- Gorda, T., Kurkela, A., Romatschke, P., Säppi, S., & Vuorinen, A. 2018, Phys. Rev. Lett., 121, 202701, doi: [10.1103/PhysRevLett.121.202701](https://doi.org/10.1103/PhysRevLett.121.202701)
- Hebeler, K., Lattimer, J. M., Pethick, C. J., & Schwenk, A. 2013, The Astrophysical Journal, 773, 11, doi: [10.1088/0004-637X/773/1/11](https://doi.org/10.1088/0004-637X/773/1/11)
- Hinderer, T., Lackey, B. D., Lang, R. N., & Read, J. S. 2010, Phys. Rev. D, 81, 123016, doi: [10.1103/PhysRevD.81.123016](https://doi.org/10.1103/PhysRevD.81.123016)
- Keller, J., Wellenhofer, C., Hebeler, K., & Schwenk, A. 2021, Phys. Rev. C, 103, 055806, doi: [10.1103/PhysRevC.103.055806](https://doi.org/10.1103/PhysRevC.103.055806)
- Kingma, D. P., & Ba, J. 2014, Adam: A Method for Stochastic Optimization, arXiv, doi: [10.48550/ARXIV.1412.6980](https://doi.org/10.48550/ARXIV.1412.6980)
- Kojo, T. 2021, AAPPs Bulletin, 31, 11, doi: [10.1007/s43673-021-00011-6](https://doi.org/10.1007/s43673-021-00011-6)
- Komoltsev, O., & Kurkela, A. 2022, Phys. Rev. Lett., 128, 202701, doi: [10.1103/PhysRevLett.128.202701](https://doi.org/10.1103/PhysRevLett.128.202701)

- Krastev, P. G. 2022, *Galaxies*, 10,
doi: [10.3390/galaxies10010016](https://doi.org/10.3390/galaxies10010016)
- Kurkela, A., Romatschke, P., & Vuorinen, A. 2010, *Phys. Rev. D*, 81, 105021, doi: [10.1103/PhysRevD.81.105021](https://doi.org/10.1103/PhysRevD.81.105021)
- Lattimer, J. M., & Prakash, M. 2004, *Science*, 304, 536,
doi: [10.1126/science.1090720](https://doi.org/10.1126/science.1090720)
- Lim, Y., & Holt, J. W. 2019, *The European Physical Journal A*, 55, 209, doi: [10.1140/epja/i2019-12917-9](https://doi.org/10.1140/epja/i2019-12917-9)
- Miller, M. C., Lamb, F. K., Dittmann, A. J., et al. 2019, *The Astrophysical Journal Letters*, 887, L24,
doi: [10.3847/2041-8213/ab50c5](https://doi.org/10.3847/2041-8213/ab50c5)
- Miller, M. C., Lamb, F. K., Dittmann, A. J., et al. 2021, *ApJL*, 918, L28, doi: [10.3847/2041-8213/ac089b](https://doi.org/10.3847/2041-8213/ac089b)
- Morawski, F., & Bejger, M. 2020, *A&A*, 642, A78,
doi: [10.1051/0004-6361/202038130](https://doi.org/10.1051/0004-6361/202038130)
- Most, E. R., Weih, L. R., Rezzolla, L., & Schaffner-Bielich, J. 2018, *Phys. Rev. Lett.*, 120, 261103,
doi: [10.1103/PhysRevLett.120.261103](https://doi.org/10.1103/PhysRevLett.120.261103)
- Oppenheimer, J. R., & Volkoff, G. M. 1939, *Phys. Rev.*, 55, 374, doi: [10.1103/PhysRev.55.374](https://doi.org/10.1103/PhysRev.55.374)
- Raaijmakers, G., Greif, S. K., Hebeler, K., et al. 2021, *The Astrophysical Journal Letters*, 918, L29,
doi: [10.3847/2041-8213/ac089a](https://doi.org/10.3847/2041-8213/ac089a)
- Raithel, C. A., Özel, F., & Psaltis, D. 2017, *ApJ*, 844, 156,
doi: [10.3847/1538-4357/aa7a5a](https://doi.org/10.3847/1538-4357/aa7a5a)
- Riley, T. E., Watts, A. L., Bogdanov, S., et al. 2019, *ApJL*, 887, L21, doi: [10.3847/2041-8213/ab481c](https://doi.org/10.3847/2041-8213/ab481c)
- Riley, T. E., Watts, A. L., Ray, P. S., et al. 2021, *The Astrophysical Journal Letters*, 918, L27,
doi: [10.3847/2041-8213/ac0a81](https://doi.org/10.3847/2041-8213/ac0a81)
- Shuryak, E. V. 1980, *Physics Reports*, 61, 71,
doi: [https://doi.org/10.1016/0370-1573\(80\)90105-2](https://doi.org/10.1016/0370-1573(80)90105-2)
- Soma, S., Wang, L., Shi, S., Stöcker, H., & Zhou, K. 2022, *Journal of Cosmology and Astroparticle Physics*, 2022, 071, doi: [10.1088/1475-7516/2022/08/071](https://doi.org/10.1088/1475-7516/2022/08/071)
- Tews, I., Krüger, T., Hebeler, K., & Schwenk, A. 2013, *Phys. Rev. Lett.*, 110, 032504,
doi: [10.1103/PhysRevLett.110.032504](https://doi.org/10.1103/PhysRevLett.110.032504)
- Valentim, R., Rangel, E., & Horvath, J. E. 2011, *Monthly Notices of the Royal Astronomical Society*, 414, 1427,
doi: [10.1111/j.1365-2966.2011.18477.x](https://doi.org/10.1111/j.1365-2966.2011.18477.x)
- Witten, E. 1984, *Phys. Rev. D*, 30, 272,
doi: [10.1103/PhysRevD.30.272](https://doi.org/10.1103/PhysRevD.30.272)
- Zhang, N.-B., Li, B.-A., & Xu, J. 2018, *The Astrophysical Journal*, 859, 90, doi: [10.3847/1538-4357/aac027](https://doi.org/10.3847/1538-4357/aac027)